DOI: 10.31276/VJSTE.2024.0118

Hydrogen spillover on Ni-, Pd- and Pt-doped ZnO ultra-thin films: A density functional theory study

Ho Viet Thang*

University of Science and Technology, The University of Da Nang, 54 Nguyen Luong Bang Street, Lien Chieu Ward, Da Nang City, Vietnam

Received 3 November 2024; revised 2 December 2024; accepted 16 March 2025

Abstract:

Hydrogen spillover plays an important role in heterogeneous catalytic reactions, such as syngas production, hydrogen production, and CO_2 conversion. Among metal oxide materials, ZnO films stand out as promising candidates for hydrogen storage, though their pure form has limitations for certain applications. In this study, the hydrogen spillover on Ni, Pd, and Pt-doped ZnO ultra-thin films is investigated by employing the DFT+U method. To this end, the spillover and non-spillover structures of hydrogen are considered, and their electronic structures are evaluated in undoped and doped ZnO ultra-thin films. The calculated results show that the Ni, Pd, and Pt-doped ZnO ultra-thin films can alter the electronic properties of the undoped material from insulating to metallic characteristics. While hydrogen spillover cannot occur on undoped ZnO films, it can proceed with 50% coverage of H atoms on Pd-doped ZnO films and 100% hydrogen coverage on Ni- and Pt-doped ZnO films. This study paves the way for synthesising ZnO-based catalysts for hydrogen storage, catalysis, and other desired applications.

Keywords: **adsorption, catalysis, density functional theory, hydrogen spillover, ZnO films.**

Classification numbers: **2.1, 2.2, 2.3**

1. Introduction

Zinc oxide (ZnO) is a versatile semiconductor material with a wide range of applications in optoelectronics, sensors, and energy storage [1]. ZnO exists in various forms, including bulk (3D) materials, 2D structures, nanowires, nanobelts [2, 3]. Recently, two-dimensional (2D) ZnO with a monolayer, known as an ultra-thin film, has attracted significant attention due to its unique properties and potential applications [4]. ZnO ultra-thin films can be produced through various methods, including exfoliation of bulk ZnO crystals and chemical vapor deposition on suitable substrates [5, 6]. This film can be successfully synthesised in a free-standing form [7]. However, pure ZnO films are limited in certain applications that require higher charge carrier concentrations. To achieve the desired applications, doping with heteroatoms is a promising approach. For instance, doping with gallium (Ga), indium (In), and aluminium (Al) can enhance n-type, while doping with lithium (Li), sodium (Na), and potassium (K) can convert materials to p-type. Additionally, doping with equivalent metals such as copper (Cu) can reduce the band gap, making the material suitable for adsorption and catalysis [8-10].

Among the important applications, ZnO materials have been utilised in various catalytic processes, such as CO_2 conversion, hydrogen production, and methanol production, in which hydrogen spillover processes play a crucial role [11, 12]. The hydrogen spillover process involves several sequential steps. Initially, hydrogen molecules adsorb and dissociate onto the supported metal surface (hydrogen non-spillover). These hydrogen atoms subsequently migrate and diffuse onto the support (hydrogen spillover), ultimately leading to the storage of hydrogen [13]. These steps are related to the energetic stability of hydrogen non-spillover and hydrogen spillover. However, on pristine ZnO, the hydrogen spillover process is limited and cannot occur [9]. To enhance hydrogen spillover, metals can be deposited onto ZnO ultra-thin films [14]. This approach can overcome the limitations of pristine ZnO and promote the formation of the hydrogen spillover process, thereby enhancing the catalytic activity of ZnO films. Among supported metals, Ni, Pd, and Pt are the most promising candidates for promoting hydrogen spillover processes [15]. However, the use of these metals results in inefficient utilisation and high costs due to their large particle size. Therefore, reducing the particle size of the metal to the smallest possible dimensions aims to achieve the highest utilisation efficiency. However, stabilising small-sized metals on the support requires different techniques due to the metals' high surface energy, which leads to diffusion and aggregation. Doping metals onto supports is a promising approach to overcome these challenges and achieve efficient metal utilisation as well as high selectivity [16]. In these materials, single metal-doped atoms serve as active centres for adsorption and catalysis.

*Email: hvthang@dut.udn.vn

However, there is a lack of information regarding the nature of metals doped onto ultra-thin ZnO films for hydrogen spillover.

In this study, the hydrogen spillover on M (M=Ni, Pd, Pt) doped ZnO ultra-thin films is theoretically investigated using the DFT+U method. A range of hydrogen atom numbers, from the lowest coverage (1H) to saturated coverage, is considered. While the spillover process on Ni- and Pt-doped ZnO ultra-thin films occurs when the number of adsorbed hydrogen atoms reaches saturation, hydrogen spillover can occur on Ni-doped ZnO ultra-thin films with 50% hydrogen coverage. This study demonstrates that hydrogen spillover on ZnO ultra-thin films can be applied to other doped metals and for further desired applications.

2. Computational methods and models

The computational calculations were carried out by using the Quantum Espresso software suite v.7.3.1 [17-19]. The exchange-correlation functional was approximated by using the generalised gradient approximation (GGA) within the Perdew, Burke, and Ernzerhof (PBE) functional [20]. The interaction of ions and core electrons was evaluated employing the GBRV ultrasoft pseudopotential [21]. The valence electrons were explicitly characterised as Zn(2s, 3p, 3d, 4s), O(3s, 3p), Ni(2s, 3p, 3d, 4s) , Pd(2s, 3p, 3d, 4s), Pt(2s, 3p, 3d, 4s), H(1s). To partly compensate for the lack of accuracy of PBE method, the author used DFT+U approach [22], in which U parameters were set of 10 and 7 eV for 3d Zn and 2p O, respectively [9]. The U parameters can effectively reproduce the cell parameters and electronic band gap of bulk wurtzite ZnO, which is in good agreement with experimental data. In particular, the calculated band gap is 3.13 eV, while the experimental band gap is 3.37 eV [23]. Calculated and experimental cell parameters are a=b=3.268 Å and c=5.2281Å, a=b=3.255 Å and c=5.207 Å, respectively [24]. The U value does not apply to doped metals; the effect is negligible, as mentioned in a previous study [10]. A k-point mesh of 3×3×1 was used to sample the Brillouin zone. The convergence threshold for self-consistency is set to 10^{-8} Ry. A plane-wave kinetic energy cutoff of 40 Ry and Gaussian smearing technique were used to facilitate Brillouin Zone integration.

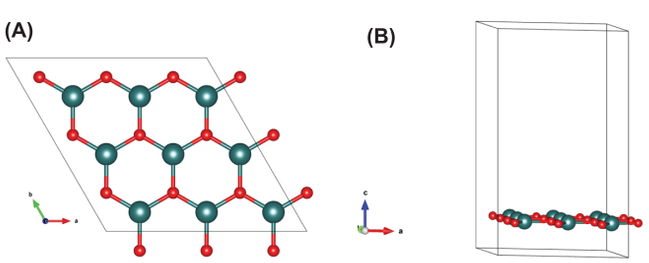

Fig. 1. (A) Top view and (B) side view of monolayer ZnO where Zn and O are green and red spheres, respectively.

ZnO ultra-thin film models adopted a (3×3) supercell of a monoatomic layer, creating a vacuum of 15 Å to avoid interaction between layers (Fig. 1). A Zn lattice cation was replaced by an M atom (M=Ni, Pd, Pt) in the doped ZnO ultra-thin film models. This corresponds to about 11% wt. of doping, which has been found in previous studies [10, 25]. The adsorption energies per H atom ($E_{ads/H}$ in eV) were computed by Equation (1):

$$E_{ads/H} = (E(nH/S) - E(S) - n*E(H))/n \quad (1)$$

where E(nH/S), E(S), and E(H) are total energies (eV) of the adsorption complexes of nH on ZnO films, M-doped ZnO films, and the H atom, respectively, and n is the number of H atoms.

The difference in adsorption energies between spillover and non-spillover configurations (ΔE in units of eV) of n number of H atoms adsorption on M-doped ZnO ultra-thin films is calculated by Equation (2):

$$\Delta E = E_{(ads/H)sp} - E_{(ads/H)nonsp} \quad (2)$$

where $E_{(ads/H)sp}$ and $E_{(ads/H)nonsp}$ are the adsorption energies per H atom (eV) of spillover and non-spillover configurations, respectively.

The effective charge of the atoms was evaluated by employing the Bader method [26-28].

3. Results and discussion

3.1. The electronic characteristics of Ni, Pd, Pt doped ZnO ultra-thin films

First, the author evaluated the electronic properties of undoped ZnO ultra-thin films. The ZnO ultra-thin film was obtained by cutting a monolayer of ZnO from the (001) plane of bulk wurtzite ZnO. Unlike bulk ZnO, where Zn and O localise on distinct planes, the Zn and O reside in the same plane with an identical Zn-O bond length of 1.89 Å (Table 1) and a Zn-O-Zn bond angle of 120°, forming a graphitic-like structure (Fig. 1). In other words, the Zn and O bond via sp^2 hybridisation in ZnO ultra-thin films, compared to sp^3 hybridisation in bulk ZnO. However, the band gap is reduced from 3.21 eV in bulk to 1.96 eV in ultra-thin film ZnO. This indicates that the ZnO ultra-thin film still exhibits insulating character. To evaluate the oxidation state of Zn in ultra-thin film ZnO and the doped metal, the author computed the Bader charge of these cations. It is clear that the oxidation state of Zn in undoped ZnO ultra-thin films is +2, corresponding to a Bader charge of +1.21 |e|. Note that the Bader charge of cations is qualitative to the oxidation state of cations and can be used to evaluate the formal oxidation state of cations [29]. Furthermore, the undoped ZnO ultra-thin film exhibits non-magnetic behaviour, similar to bulk ZnO, as indicated by a magnetic moment of 0.00 μ_B (Table 1) and a symmetric density of states (DOS) for spin-up and spin-down (Fig. 2A).

Table 1. The characteristics of the M (M=Zn, Ni, Pd, Pt) -doped ZnO ultra-thin films, band gap (E_g), average bond length between single atom M and O (d(M-O)), Bader charge of M (Q(M)), and magnetic moment (Mag.).

System	E_g (eV)	d(M-O) (Å)	Q(M) (|e|)	Mag. (μ_B)
ZnO	1.96	1.89, 1.89, 1.89	1.21	0.00
Ni-doped ZnO	0.45	1.86, 1.86, 1.86	1.16	2.00
Pd-doped ZnO	0.00	2.00, 2.00, 2.00	0.95	2.00
Pt-doped ZnO	0.00	2.00, 2.00, 2.00	0.97	2.00

When Zn is substituted by Ni, the Ni-O bond length is slightly truncated by 0.03 Å compared to the corresponding Zn-O bond length of undoped ZnO (Table 1). This is due to the radius of Ni^{2+} (0.078 Å) being smaller than that of Zn^{2+} (0.083 Å) [30]. Furthermore, the smaller radius of Ni^{2+} results in a slightly smaller Bader charge of Ni^{2+} in doped ZnO (1.16 |e|) compared to 1.21 |e| for Zn. This also leads to a lowering of the valence band and a reduction in the band gap by 1.51 eV with respect to undoped ZnO ultra-thin films (Table 1, Fig. 2A). Unlike undoped ZnO films, the Ni-doped ZnO films exhibit magnetic behaviour, with a magnetic

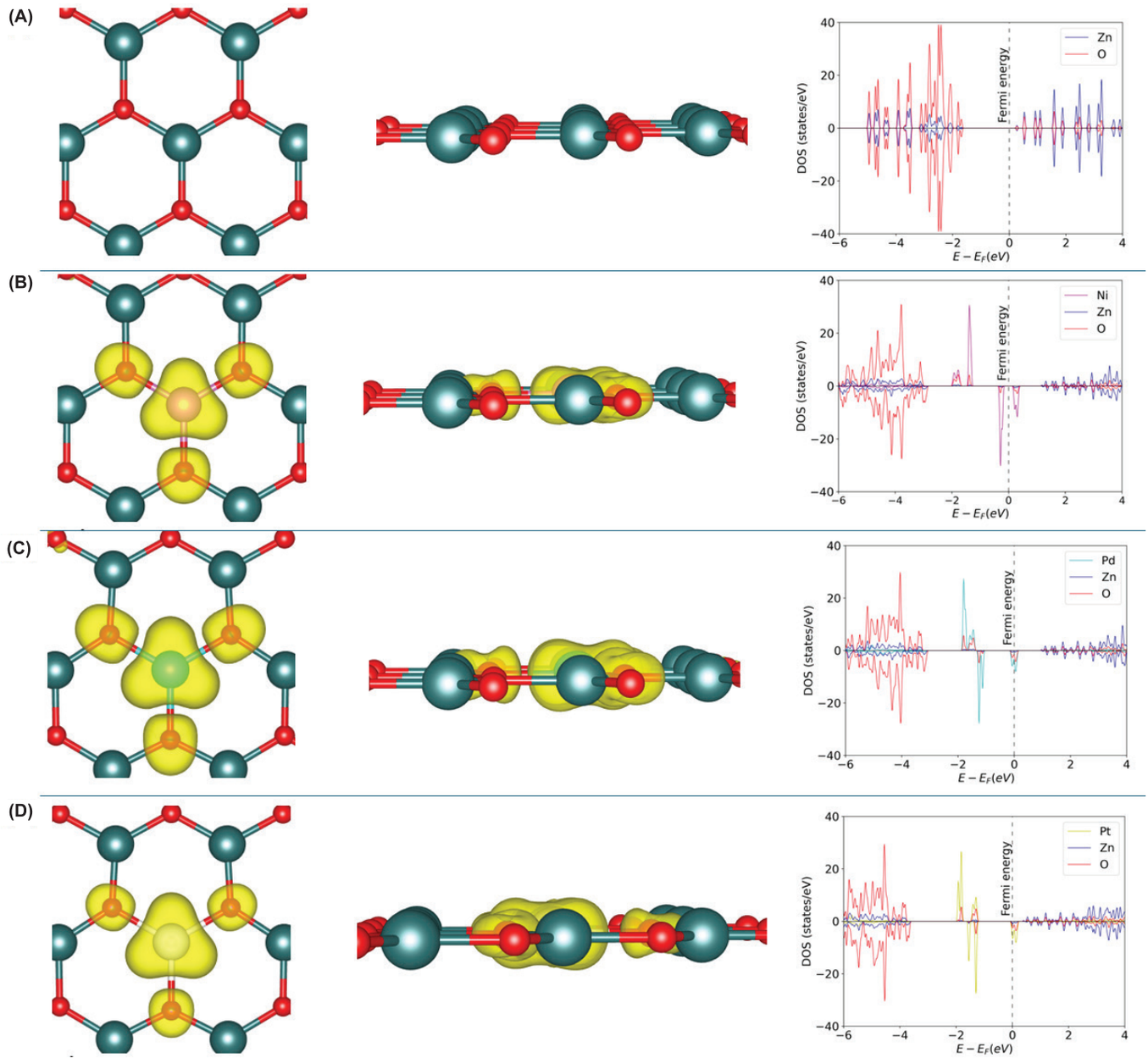

Fig. 2. Top view (left), side view (middle), and density of states profiles (right) of (A) undoped ZnO, (B) Ni-doped ZnO, (C) Pd-doped ZnO, (D) Pt-doped ZnO ultra-thin films. Zn, O, Ni, Pd, Pt are green, red, pink, light blue, and white spheres, respectively. The transparent yellow clouds are the spin density with a surface value of 0.003 |e|.bohr^{-3}.

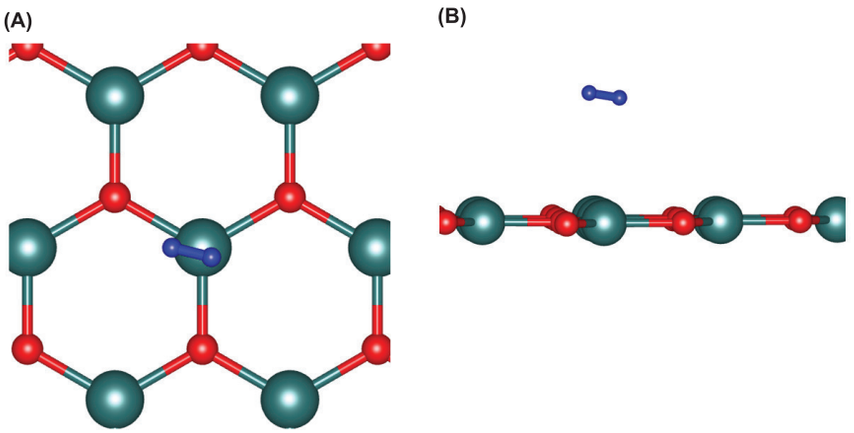

Fig. 3. (A) Top view and (B) side view of H_2 adsorbed on ZnO ultra-thin films. Zn, O, and H are green, red, and blue spheres, respectively.

moment of 2.00 μ_B (Table 1). The magnetic properties of Ni-doped ZnO films are illustrated by spin density and DOS profiles (Fig. 2B).

Considering Pd- and Pt-doped ZnO ultra-thin films, similar electronic structures were observed, in which the Pd-O or Pt-O bond length is 2.00 Å, and the Bader charges are 0.95 and 0.97 (|e|), respectively, with a magnetic moment of 2.00 μ_B. This is also confirmed by the spin density and DOS profiles for doped Pd and doped Pt (Figs. 2C, 2D). However, the Pd- and Pt-doped materials exhibit metallic properties, as indicated by the presence of the DOS crossing the Fermi level (Figs. 2C, 2D). This is due to the strong interaction between the Pd- and Pt-doped metals and the framework oxygen atoms, compared to that of Ni-doped ZnO (see DOS profile in Fig. 2). This interaction also leads to the lowering of the valence bands of ZnO ultra-thin films with respect to undoped ZnO ultra-thin films.

3.2. nH adsorption on Ni, Pd, and Pt doped ZnO ultra-thin films

For comparison, the author evaluated the hydrogen spillover process on undoped ZnO ultra-thin films. To this end, the author considered the adsorption of 2H in undoped ZnO via both non-spillover and spillover structures. However, the 2H atoms spontaneously form H_2 and reside at a considerable distance from the ZnO films (3.023 Å), as shown in Fig. 3. This indicates that the undoped ZnO ultra-thin films are unable to adsorb nH in either spillover or non-spillover configurations.

On M (M=Ni, Pd, Pt) -doped ZnO ultra-thin films, the author considered 1H, 2H, and 4H adsorbed on the doped M site with non-spillover structures (nH bound to the M site) and spillover structures ((n-1) H bound to the M site and 1H bound to the supporting ZnO films in the vicinity of the doped M). The author also considered 6H adsorbed on the doped M site, but either structure forms H_2 molecules or remains unbound on the M sites. This demonstrates that the saturated coverage of nH on doped M sites is 4, corresponding to 100%.

On Ni-doped ZnO ultra-thin films, H is bound to Ni with a Ni-H bond length of 1.54 Å and H is bound to framework O with an O-H bond length of 0.94 Å for spillover structures (Fig. 4). The adsorption energy per H atom via non-spillover and spillover configurations increases in magnitude from |-2.54| to |-3.02| eV and from |-1.93| to |-3.05| eV, respectively, when the number of nH increases from 1 to 4 (Table 1). The increasing adsorption energy per H atom is associated with the decreasing Bader charge of doped Ni as nH increases in both non-spillover and spillover configurations (Table 2). This is due to the charge transfer from nH to doped Ni, indicated by the slightly positive charge of nH. As the author can see, the adsorption energy per H atom of non-spillover structures is stronger than that of spillover configurations when the number of nH atoms is less than 4. In particular,

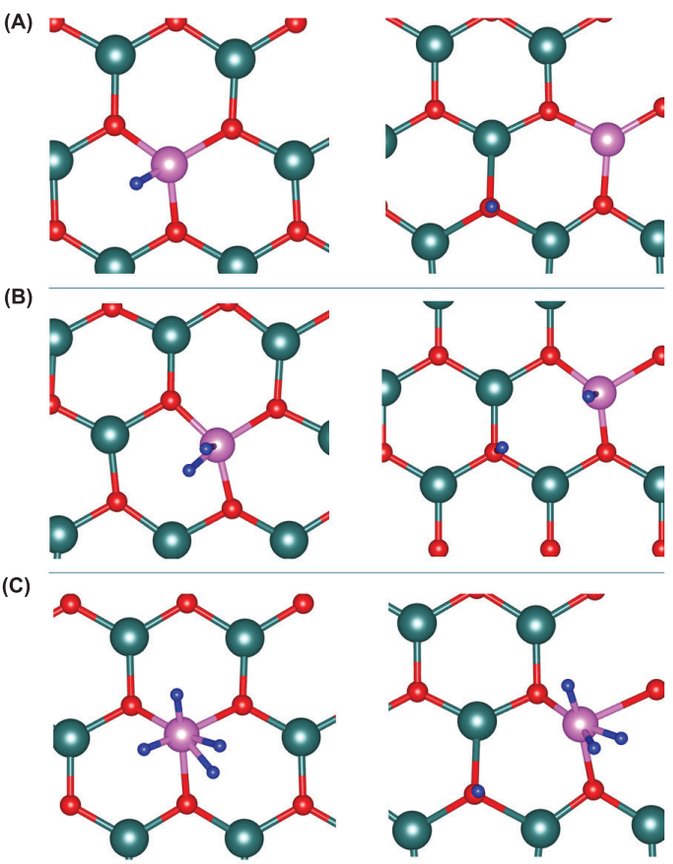

Fig. 4. Non-spillover (left) and spillover (right) structures of (A) 1H, (B) 2H, and (C) 4H atoms adsorbed on Ni-doped ZnO ultrathin films. Zn, O, Ni, H are green, red, purple, and blue spheres, respectively.

Table 2. Adsorption energies per H atom ($E_{ads/H}$) of non-spillover and spillover structures. Bader charge of M (M=Ni, Pd, Pt) -doped ZnO ultra-thin films, of total non-spillover H atoms adsorbed on doped M (Q, nH on M), of total spillover H atoms adsorbed on doped M (Q, (n-1)H on M), of spillover H on ZnO (Q, H on ZnO); the different energies between spillover and non-spillover configurations (ΔE) of nH atoms adsorption on M doped ZnO ultra-thin films.

nH	Non-spillover			Spillover				$\Delta E_{ads/H}$ (eV)
	$E_{ads/H}$ (eV)	*Q, M* (|e|)	*Q, nH on M* (|e|)	$E_{ads/H}$ (eV)	*Q, Ni* (|e|)	*Q, (n-1)H on M* (|e|)	*Q, H on ZnO* (|e|)	
Ni:ZnO								
1H	-2.54	1.12	-0.02	-1.93	0.97	-	1.00	0.61
2H	-2.72	1.09	0.02	-2.30	0.94	-0.16	1.00	0.41
4H	-3.02	0.96	0.14	-3.05	0.77	-0.10	1.00	-0.03
Pd:ZnO								
1H	-3.37	0.93	-0.01	-3.11	0.59	-	1.00	0.26
2H	-3.43	0.90	0.12	-3.49	0.65	-0.10	1.00	-0.06
4H	-3.46	0.86	0.22	-3.52	0.58	-0.03	1.00	-0.06
Pt:ZnO								
1H	-4.15	0.91	-0.03	-3.42	0.53	-	1.00	0.73
2H	-3.99	0.85	0.09	-3.86	0.61	-0.07	1.00	0.13
4H	-3.91	0.90	0.18	-4.01	0.70	-0.18	1.00	-0.10

the difference in adsorption energy per H atom between spillover and non-spillover configurations for 1H and 2H atoms is 0.61 and 0.41 eV, respectively. When the number of nH atoms exceeds 2, the difference in adsorption energy per H atom between spillover and non-spillover configurations becomes negative (-0.03 eV). This indicates that hydrogen spillover on Ni-doped ZnO ultra-thin films can occur with nH greater than 2.

Similar to that on Ni-doped ZnO, H is bound to Pd with an average bond length of 1.53 Å and bound to framework O with a bond length of 0.97 Å in the case of spillover on Pd-doped ZnO (Fig. 5). However, the adsorption energy per H atom on Pd-doped ZnO ultra-thin films is stronger than that on Ni-doped ZnO by a range of 0.4 to 0.8 eV in magnitude (Table 2). The adsorption energy per H atom in magnitude also increases with the number of H atoms in both non-spillover and spillover structures. In particular, the adsorption energy per H atom increases from |-3.37| eV for 1H to |-3.46| eV for 4H atoms in non-spillover structures and from |-3.11| to |-3.52| eV in spillover structures (Table 2). However, the difference in adsorption energy per H atom between spillover and non-spillover configurations is negative (-0.06 eV) when the number of H atoms exceeds 2. The spillover process can occur on Pd-doped ZnO ultra-thin films with a number of H atoms less than that in Ni-doped ZnO ultra-thin films (4H).

Regarding hydrogen non-spillover and spillover on Pt-doped ZnO ultra-thin films, H is bound to Pt with an H-Pt bond length of 1.54 Å and bound to framework O with an H-O bond length of 0.96 Å (Fig. 6). Furthermore, the adsorption energy per H atom in magnitude for the non-spillover configuration is reduced from |-4.15| eV for 1H

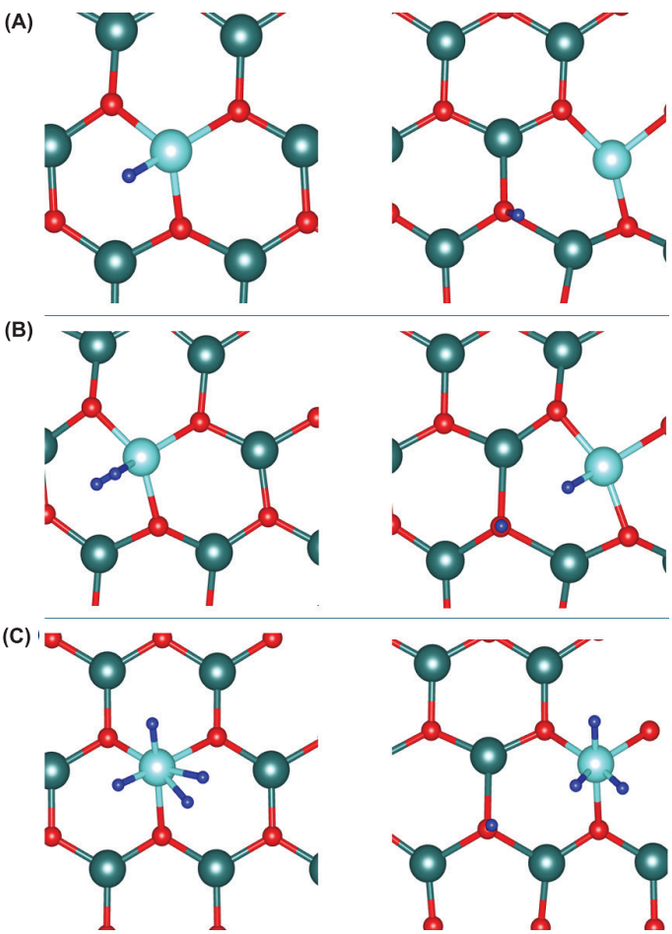

Fig. 5. Non-spillover (left) and spillover (right) structures of (A) 1H, (B) 2H, and (C) 4H atoms adsorbed on Pd-doped ZnO ultra-thin films. Zn, O, Pd, H are green, red, light blue, and blue spheres, respectively.

to |-3.91| eV for 4H, while this trend is observed in the opposite direction for spillover configurations, where the adsorption energy per H atom increases from |-3.42| eV for 1H to |-4.01| eV for 4H (Table 2).

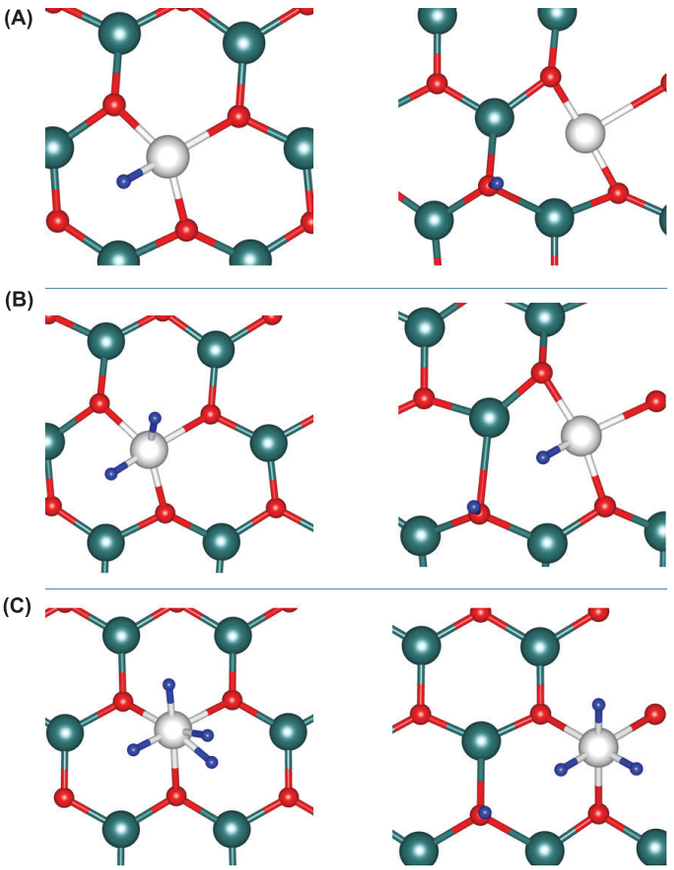

Fig. 6. Non-spillover (left) and spillover (right) structures of (A) 1H, (B) 2H, and (C) 4H atoms adsorbed on Pt-doped ZnO ultra-thin films. Zn, O, Pt, H are green, red, white, and blue spheres, respectively.

The difference in the trend of adsorption energy per H atom on Pt-doped ZnO ultra-thin films can be explained by the deformation of structures. While the non-spillover configuration mostly leaves the ZnO structures unchanged, a large local deformation of the ZnO structures is observed, in which the symmetry of the hexagonal structure of Pt is broken, as indicated by the difference in Pt-O bond length (Fig. 6). However, the spillover of H can be observed on Pt-doped ZnO ultra-thin films when the number of H atoms exceeds 2 (Table 2).

In all M-doped ZnO ultra-thin films, the Bader charge of H is negative for 1H, turning into a positive charge, indicating that charge transfer occurs from doped M to H in non-spillover configurations for 1H. The positive charge of H is found in the spillover configurations, which is due to the charge transfer from H to ZnO films when H spillover occurs, illustrated by a positive charge of +1 |e| (Table 2). The results demonstrate the different nature of the metals, causing variations in hydrogen adsorption and spillover processes.

4. Conclusions

The author has investigated the hydrogen spillover process on M-doped (M=Ni, Pd, Pt) ZnO ultra-thin films using the DFT+U method. Doping with different metals can alter the electronic properties of ZnO films. In particular, Ni doping reduces the band gap of the ZnO film, while Pd and Pt doping results in metallic characteristics for the ZnO films. In all M-doped ZnO films with saturated H coverage, the spillover process was observed. However, hydrogen spillover was noted on Ni- and Pt-doped ZnO films with a saturated coverage of adsorbed H atoms (100%), while hydrogen spillover on Pd-doped ZnO films occurred at a lower coverage of adsorbed H atoms (50%). Conversely, hydrogen spillover was not observed on undoped ZnO films. This finding suggests that, in terms of H spillover, Pd-doped ZnO ultra-thin films exhibit a stronger preference than Ni- and Pt-doped ZnO ultra-thin films.

COMPETING INTERESTS

The author declares that there is no conflict of interest regarding the publication of this article.

REFERENCES

[1] Ü. Özgür, Y.I. Alivov, C. Liu, et al. (2005), "A comprehensive review of ZnO materials and devices", *Journal of Applied Physics*, **98(4)**, DOI: 10.1063/1.1992666.

[2] A. Moumen, N. Kaur, N. Poli, et al. (2020), "One dimensional ZnO nanostructures: Growth and chemical sensing performances", *Nanomaterials*, **10(10)**, DOI: 10.3390/nano10101940.

[3] J. Hu, N. You, Z. Yu, et al. (2016), "Two-dimensional ZnO ultrathin nanosheets decorated with Au nanoparticles for effective photocatalysis", *Journal of Applied Physics*, **120(7)**, DOI: 10.1063/1.4961036.

[4] Q. Pan, B.H. Liu, M.E. McBriarty, et al. (2014), "Reactivity of ultra-thin ZnO films supported by Ag(111) and Cu(111): A comparison to ZnO/Pt(111)", *Catal. Lett.*, **144(4)**, pp.648-655, DOI: 10.1007/s10562-014-1191-y.

[5] J.F. Lei, Z.W. Wang, W.S. Li (2014), "Controlled fabrication of ordered structure-based ZnO films by electrochemical deposition", *Thin Solid Films*, **573**, pp.74-78, DOI: 10.1016/j.tsf.2014.11.009.

[6] L. Znaidi (2010), "Sol-gel-deposited ZnO thin films: A review", *Materials Science and Engineering: B*, **174(1)**, pp.18-30, DOI: 10.1016/j.mseb.2010.07.001.

[7] Z. Wang, L. Gan, H. He, et al. (2017), "Free-standing atomically thin ZnO layers via oxidation of zinc chalcogenide nanosheets", *ACS Appl. Mater. Interfaces*, **9(15)**, pp.13537-13543, DOI: 10.1021/acsami.7b02425.

[8] S. Horzum, E. Bulduk, D. Şener, et al. (2021), "Comparison of characteristic properties of Al, Ga, and in-doped ZnO thin films formed by sol-gel method", *Superlattices and Microstructures*, **159**, DOI: 10.1016/j.spmi.2021.107034.

[9] H.V. Thang (2023), "A DFT+U study of CO and H_2 adsorption properties on Ga, Li, and Cu doped ZnO surfaces", *Chem. Nano Mat.*, **9(6)**, DOI: 10.1002/cnma.202300024.

[10] H.V. Thang, G. Pacchioni (2019), "Electronic structure of Al, Ga, In and Cu doped ZnO/Cu(111) bilayer films", *Physical Chemistry Chemical Physics*, **21(1)**, pp.369-377, DOI: 10.1039/C8CP06717A.

[11] P. Borisut, A. Nuchitprasittichai (2019), "Methanol production via CO_2 hydrogenation: Sensitivity analysis and simulation-based optimization", *Frontiers in Energy Research*, **7**, DOI: 10.3389/fenrg.2019.00081.

[12] S. Kattel, P.J. Ramírez, J.G. Chen, et al. (2017), "Active sites for CO_2 hydrogenation to methanol on Cu/ZnO catalysts", *Science*, **355(6331)**, pp.1296-1299, DOI: 10.1126/science.aal3573.

[13] M. Xiong, Z. Gao, Y. Qin (2021), "Spillover in heterogeneous catalysis: New insights and opportunities", *ACS Catal*., **11(5)**, pp.3159-3172, DOI: 10.1021/acscatal.0c05567.

[14] A. Sihag, Z.L. Xie, H.V. Thang, et al. (2019), "DFT insights into comparative hydrogen adsorption and hydrogen spillover mechanisms of Pt_4/Graphene and Pt_4/Anatase (101) surfaces", *J. Phys. Chem. C*, **123(42)**, pp.25618-25627, DOI: 10.1021/acs.jpcc.9b04419.

[15] J.H. Guo, D.D. Liu, X.D. Li, et al. (2018), "Pt_4, Pd_4, Ni_4, and Ti_4 catalyzed hydrogen spillover on penta-graphene for hydrogen storage: The first-principles and kinetic Monte Carlo study", *International Journal of Hydrogen Energy*, **43(4)**, pp.2247-2255, DOI: 10.1016/j.ijhydene.2017.11.169.

[16] H. Jin, P. Li, P. Cui, et al. (2022),"Unprecedentedly high activity and selectivity for hydrogenation of nitroarenes with single atomic Co_1-N_3P_1 sites", *Nat. Commun.*, **13(1)**, DOI: 10.1038/s41467-022-28367-9.

[17] P. Giannozzi, S. Baroni, N. Bonini, et al. (2009), "QUANTUM ESPRESSO: A modular and open-source software project for quantum simulations of materials", *J. Phys.: Condens. Matter.*, **21(39)**, DOI: 10.1088/0953-8984/21/39/395502.

[18] P. Giannozzi, O. Andreussi, T. Brumme, et al. (2017), "Advanced capabilities for materials modelling with Quantum ESPRESSO", *J. Phys.: Condens. Matter.*, **29(46)**, DOI: 10.1088/1361-648X/aa8f79.

[19] P. Giannozzi, O. Baseggio, P. Bonfà, et al. (2020), "Quantum ESPRESSO toward the exascale", *The Journal of Chemical Physics*, **152(15)**, DOI: 10.1063/5.0005082.

[20] J.P. Perdew, K. Burke, M. Ernzerhof (1996), "Generalized gradient approximation made simple", *Phys. Rev. Lett.*, **77(18)**, pp.3865-3868, DOI: 10.1103/PhysRevLett.77.3865.

[21] K.F. Garrity, J.W. Bennett, K.M. Rabe, et al. (2014), "Pseudopotentials for high-throughput DFT calculations", *Computational Materials Science*, **81**, pp.446-452, DOI: 10.1016/j.commatsci.2013.08.053.

[22] S.L. Dudarev, G.A. Botton, S.Y. Savrasov, et al. (1998), "Electron-energy-loss spectra and the structural stability of nickel oxide: An LSDA+U study", *Phys. Rev. B*, **57(3)**, pp.1505-1509, DOI: 10.1103/PhysRevB.57.1505.

[23] A. Mang, K. Reimann, S. Rübenacke (1995), "Band gaps, crystal-field splitting, spin-orbit coupling, and exciton binding energies in ZnO under hydrostatic pressure", *Solid State Communications*, **94(4)**, pp.251-254, DOI: 10.1016/0038-1098(95)00054-2.

[24] H. Ullah, A. Iqbal, M. Zakria, et al. (2015),"Structural and spectroscopic analysis of wurtzite $(ZnO)_1$-x(Sb_2O_3)x composite semiconductor", *Progress in Natural Science: Materials International*, **25(2)**, pp.131-136, DOI: 10.1016/j.pnsc.2015.02.003.

[25] V.A. Owoeye, E. Ajenifuja, E.A. Adeoye, et al. (2019), "Microstructural and optical properties of Ni-doped ZnO thin films prepared by chemical spray pyrolysis technique", *Mater. Res. Express*, **6(8)**, DOI: 10.1088/2053-1591/ab26d9.

[26] E. Sanville, S.D. Kenny, R. Smith, et al. (2007), "Improved grid-based algorithm for Bader charge allocation", *Journal of Computational Chemistry*, **28(5)**, pp.899-908, DOI: 10.1002/jcc.20575.

[27] W. Tang, E. Sanville, G. Henkelman (2009), "A grid-based Bader analysis algorithm without lattice bias", *J. Phys.: Condens. Matter.*, **21(8)**, DOI: 10.1088/0953-8984/21/8/084204.

[28] M. Yu, D.R. Trinkle (2011), "Accurate and efficient algorithm for Bader charge integration", *J. Chem. Phys.*, **134(6)**, DOI: 10.1063/1.3553716.

[29] S. Posysaev, O. Miroshnichenko, M. Alatalo, et al. (2019), "Oxidation states of binary oxides from data analytics of the electronic structure", *Computational Materials Science*, **161**, pp.403-414, DOI: 10.1016/j.commatsci.2019.01.046.

[30] H. Mekatel, S. Amokrane, A. Benturki, et al. (2012), "Treatment of polluted aqueous solutions by Ni^{2+}, Pb^{2+}, Zn^{2+}, Cr^{+6},Cd^{+2} and Co^{+2} ions by ion exchange process using faujasite zeolite", *Procedia Engineering*, **33**, pp.52-57, DOI: 10.1016/j.proeng.2012.01.1176.